Science Bulletin 63 (2018) 293–299

Contents lists available at ScienceDirect

Science Bulletin

journal homepage: www.elsevier.com/locate/scib

Science Bulletin
www.scibull.com

Article

Simulation of molecular spectroscopy with circuit quantum electrodynamics

Ling Hu [a,1], Yue-Chi Ma [a,1], Yuan Xu [a], Wei-Ting Wang [a], Yu-Wei Ma [a], Ke Liu [a], Hai-Yan Wang [a], Yi-Pu Song [a], Man-Hong Yung [b,c,*], Lu-Yan Sun [a,*]

[a] Center for Quantum Information, Institute for Interdisciplinary Information Sciences, Tsinghua University, Beijing 100084, China
[b] Institute for Quantum Science and Engineering and Department of Physics, South University of Science and Technology of China, Shenzhen 518055, China
[c] Shenzhen Key Laboratory of Quantum Science and Engineering, Shenzhen 518055, China

ARTICLE INFO

Article history:
Received 16 October 2017
Received in revised form 20 January 2018
Accepted 25 January 2018
Available online 5 February 2018

Keywords:
Molecular spectroscopy
Circuit quantum electrodynamics
Correlation function
Huang-Rhys parameter

ABSTRACT

Spectroscopy is a crucial laboratory technique for understanding quantum systems through their interactions with the electromagnetic radiation. Particularly, spectroscopy is capable of revealing the physical structure of molecules, leading to the development of the maser—the forerunner of the laser. However, real-world applications of molecular spectroscopy are mostly confined to equilibrium states, due to computational and technological constraints; a potential breakthrough can be achieved by utilizing the emerging technology of quantum simulation. Here we experimentally demonstrate through a toy model, a superconducting quantum simulator capable of generating molecular spectra for both equilibrium and non-equilibrium states, reliably producing the vibronic structure of diatomic molecules. Furthermore, our quantum simulator is applicable not only to molecules with a wide range of electronic-vibronic coupling strength, characterized by the Huang-Rhys parameter, but also to molecular spectra not readily accessible under normal laboratory conditions. These results point to a new direction for predicting and understanding molecular spectroscopy, exploiting the power of quantum simulation.

1. Introduction

Quantum simulation represents a powerful and promising means to overcome the bottleneck for simulating quantum systems with classical computers, as advocated by Feynman [1]. One of the major applications for quantum simulation is to solve molecular problems [2–8]. In recent years, much experimental progress has been achieved in simulating the electronic structures of molecules using quantum devices. Particularly, the potential energy surface of the hydrogen molecule was simulated experimentally [9–12]. However, it remains a challenge to scale up this type of experiments for larger molecules, as the phase-estimation method involved requires an enormous amount of computing resources for implementation.

An alternative and potentially more economical approach for quantum molecular simulation has been achieved by using a quantum variational approach [12–17] that aims to improve the eigenstate approximation through local measurements of the Hamiltonians. So far, most (if not all) of the molecular simulation experiments performed are all confined to the study of static properties of molecules. It is still an experimental challenge to utilize quantum simulators for studying molecular dynamics, in particular, molecular spectroscopy.

Furthermore, classical methods in predicting vibrationally-resolved absorption spectra are mostly limited in the gas phase. However, most chemical processes occur in solution, where the molecular vibrational motion depends heavily on the environment; predicting molecular spectroscopy for non-equilibrium states represents a major challenge in quantum chemistry [18].

In this work, we develop and demonstrate a quantum simulation approach for studying molecular dynamics and absorption spectroscopy using a superconducting simulator [19]. Besides simulating molecules in equilibrium, this approach of quantum simulation also allows us to obtain non-equilibrium molecular spectra that are not directly accessible under normal laboratory conditions.

In addition, it has been found that the absorption spectra of molecules [20] can be generated by Boson-Sampling [21,22] apparatus, which represents a promising approach to justify that quantum simulators cannot be simulated efficiently with any classical means. The difference is that we focus on the dynamics of the phonons, instead of the structural shift due to the Duschinsky transformation [23]. Furthermore, based on the D-Wave architecture [24], it has been proposed that the vibrational structure of a complex

* Corresponding authors.
E-mail addresses: yung@sustc.edu.cn (M.-H. Yung), luyansun@tsinghua.edu.cn (L.-Y. Sun).
[1] These authors contributed equally to this work.

https://doi.org/10.1016/j.scib.2018.02.001
2095-9273/

molecule can be mapped to an adiabatic superconducting circuit emulator, where molecular force fields have been simulated [25]. In our experiment, we instead simulate the absorption spectrum of the diatomic molecules by a hybrid digital-analog circuit model.

More specifically, our approach can be applied to obtaining the temporal correlation function of the electronic transition dipole [26,27], which yields the information about the absorption spectrum of the molecule, after applying the Fourier transformation. In our superconducting simulator, there are many adjustable control knobs for simulating the spectra for a variety of scenarios. In particular, we are able to simulate molecules in a wide range of values of the Huang-Rhys parameter D [26], which characterizes the electron-phonon coupling strength. Instead of achieving quantum supremacy, the goal of this experiment is to take a first step in showing the possibility of using superconducting devices to simulate molecular spectra.

2. Experimental background

In the following, we focus on the model approximating the electronic degrees of freedom by a two-level system (Fig. 1a). This model has been applied to study vibronic wavepacket dynamics, chemical reaction rate, Marcus theory for non-adiabatic electron transfer, etc. For molecular spectroscopy, the absorption spectra strongly depend on the initial state of the phonon degree of freedom in the manifold of the electronic ground state. In our experimental demonstration, we have performed simulations by preparing the phonon mode in pure Fock states, as well as simulations for a thermal state and a vacuum state with damping.

In all cases, we are able to experimentally observe the progression of absorption peaks separated by the vibronic frequency, which is a characteristic feature of molecular spectrum due to vibronic transitions. This flexibility of our superconducting simulator makes it a useful tool for validating theoretical prediction when scaled up. Note that in our simulation, the experiment relies on the Jaynes-Cummings interaction between a superconducting qubit and a microwave resonator, and their conditional evolution, which have been extensively studied previously (for examples, Refs. [30–33]). The novelty here is not on the experimental setup, but its application in simulating molecular spectroscopy.

The architecture of the superconducting simulator is constructed through a three-dimensional (3D) circuit quantum electrodynamics (QED) system [30,31], where a "vertical" transmon qubit is dispersively coupled to two 3D aluminum cavities for storage and readout, as shown in Fig. 1c. Alternatively, it is also possible to perform a similar simulation with trapped-ion systems [34,35]. The qubit with a transition frequency $\omega_{eg}/2\pi = 5.345$ GHz, an energy-relaxation time $T_1 = 13$ μs, and a pure dephasing time $T_\phi = 16$ μs, is used to model the electronic state $\{|g\rangle, |e\rangle\}$ of the molecule. The storage cavity (hereafter referred as the "cavity" for simplicity) is used to model the quantization of the nuclear vibrational motion, i.e., phonons $\{|0\rangle, |1\rangle, |2\rangle, \ldots\}$, with a frequency $\omega_0/2\pi = 8.230$ GHz and a lifetime $\tau_0 = 80$ μs. The cavity is well modelled as a harmonic oscillator for excitation numbers less than 30 with no need to consider the self-Kerr ($K/2\pi \approx 2$ kHz) induced by the transmon qubit.

The state-dependent frequency shift of the cavity is $\chi_{qs}/2\pi = -1.44$ MHz, allowing for a qubit-controlled operation on the cavity state. Note that the energy level of the cavity is comparable with that of the qubit, i.e., $\omega_0 \sim \omega_{eg}$. However, for a typical molecule, the phonon frequency is much smaller than that of the electronic excitation gap. Therefore, there is a general problem of frequency mismatch [36] in simulating molecules with superconducting qubits; such a challenge can be overcome by a digital or analog approach of quantum simulation [37–40].

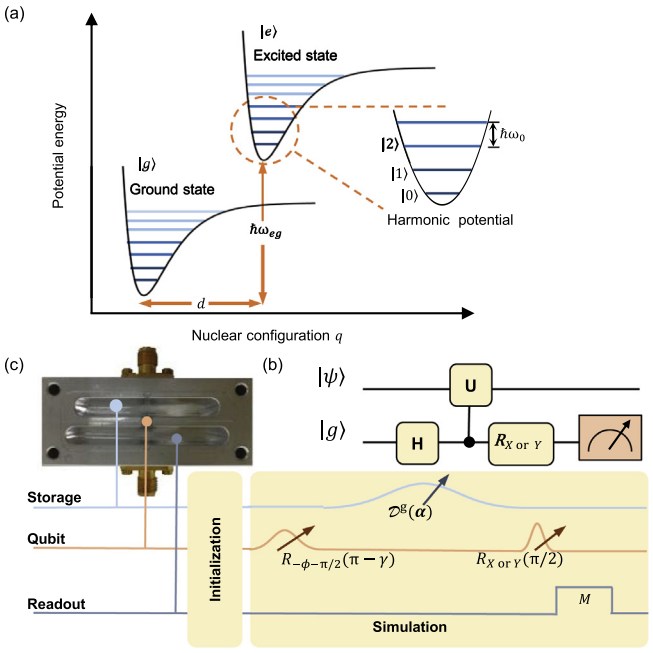

Fig. 1. Basic principle of the superconducting simulator. (a) Two identical energy surfaces of a molecule, with one curve displaced from the other along a nuclear coordinate. Near the minimum, the energy surfaces can be approximated by a harmonic potential, with an energy separation of $\hbar\omega_0$. For real molecules, the harmonic approximation is valid only for vibrational levels typically lower than 10 [28]. Therefore, we limit our simulator with small populations of high levels. Here $\hbar\omega_{eg}$ is the 0–0 energy splitting; in most cases $\omega_{eg} \gg \omega_0$. (b) The kernel quantum circuit diagram of our method to simulate diatomic molecules. The circuit consists of an ancilla qubit and a bosonic system. The bosonic system represents nuclear motion mode and is in an initial state $|\psi\rangle$. Similar to the model of deterministic quantum computation with one qubit [29], a composite evolution gate $U(t) \equiv e^{iH_g t/\hbar} e^{-iH_e t/\hbar}$ is applied to the system following a Hadamard gate on the qubit (see the main text). Finally, measurements along X and Y axis are performed to obtain the correlation function $C_{\mu\mu}(t) = \langle\sigma_x(t)\rangle + i\langle\sigma_y(t)\rangle$. (c) Device layout and pulse sequence for the superconducting simulator. A "vertical" transmon qubit (dark blue in the enlarged device schematic) on a sapphire chip (light blue) in a waveguide trench couples to two 3D Al cavities. The qubit is first prepared in the ground state $|g\rangle$ and the storage cavity (the bosonic system in (b)) is initialized to different states for various simulations (see the main text for details). As shown in (b), the simulation scheme consists of three processes: a qubit rotation $R_{-\phi-\pi/2}(\pi-\gamma)$, a controlled displacement $\mathscr{D}^g(\alpha)$ of the cavity conditional upon the qubit state $|g\rangle$, and finally a σ_x or σ_y measurement of the qubit. Here $R_\varphi(\theta)$ represents a θ–rotation along φ–axis in X-Y plane on Bloch sphere. Note that the rotation angle $\pi - \gamma$ in our simulation is not limited to $\pi/2$ (see the main text).

Together with a Josephson parametric amplifier [41,42] operating in a double-pumped mode [43,44], the readout cavity, with $\omega_m/2\pi = 7.291$ GHz and a lifetime $\tau_r = 42$ ns, is used for a high fidelity and quantum non-demolition detection of the qubit state (see the Supplementary data for details). More experimental setup details can also be found in Refs. [45,46].

3. Theoretical background

We first summarize the molecular physics involved in our work before presenting the experimental methods and results. Under the standard Born-Oppenheimer framework, the Hamiltonian $H_{\rm mol}$ of a molecule depends on the nuclear configuration $\boldsymbol{q}$ as parameters,

$$H_{\rm mol}(\boldsymbol{r}, \boldsymbol{q}) = K_e + U_{ee}(\boldsymbol{r}) + U_{eN}(\boldsymbol{r}, \boldsymbol{q}), \quad (1)$$

where K_e is the kinetic-energy term for the electrons, $U_{ee}(\boldsymbol{r})$ and $U_{eN}(\boldsymbol{r}, \boldsymbol{q})$ are the electron-electron interaction term and electron-nuclei interaction term respectively. In the low-energy sector, the molecule typically contains an electronic ground state $|g\rangle$ and an excited state $|e\rangle$, where the molecular Hamiltonian becomes [26]:

$$H_{\rm mol}(\boldsymbol{q}) = H_g(\boldsymbol{q})|g\rangle\langle g| + H_e(\boldsymbol{q})|e\rangle\langle e|, \tag{2}$$

with $H_g(\boldsymbol{q}) = K_N + V_g(\boldsymbol{q})$ and $H_e(\boldsymbol{q}) = K_N + V_e(\boldsymbol{q})$ are the nuclear energy. Here K_N is the nuclear kinetic energy, $V_g(\boldsymbol{q})$ and $V_e(\boldsymbol{q})$ are the potential energies, which are typically approximated as harmonic functions (Fig. 1a), i.e.,

$$H_g = \frac{1}{2m}p^2 + \frac{m\omega_0^2}{2}q^2, \tag{3}$$

and

$$H_e = \frac{1}{2m}p^2 + \frac{m\omega_0^2}{2}(q-d)^2 + \hbar\omega_{eg}. \tag{4}$$

Here ω_{eg} is the electronic gap between the minima of both potentials (i.e., 0–0 energy splitting).

The coupling strength between the electronic transition and the nuclear motion is characterized by the Huang-Rhys parameter, $D = \tilde{d}^2$, where $\tilde{d} = d\sqrt{m\omega_0/2\hbar}$. Similarly, the electronic transition dipole operator is given by

$$\mu(\boldsymbol{q}) = \mu_{eg}(\boldsymbol{q})|e\rangle\langle g| + \mu_{ge}(\boldsymbol{q})|g\rangle\langle e|. \tag{5}$$

However, the dependence of electronic transition moment on nuclear is usually insensitive to the nuclear motion; one can therefore approximate (known as Condon approximation) it with a constant, i.e., $\mu_{eg}(\boldsymbol{q}) = \mu_{ge}(\boldsymbol{q}) = 1$ for simplicity and $\mu(\boldsymbol{q})$ becomes a Pauli matrix σ_x, i.e., $\mu(\boldsymbol{q}) = \sigma_x$. It is reasonable to assume the electrons of molecule are initially on the ground wave function $|g\rangle$, and the time-correlation function $C_{\mu\mu}(t)$ for the dipole operator is defined by

$$C_{\mu\mu}(t) \equiv {\rm Tr}(\langle g|\sigma_x(t)\sigma_x(t=0)|g\rangle), \tag{6}$$

where $\sigma_x(t) = {\rm e}^{{\rm i}H_{\rm mol}t/\hbar}\sigma_x{\rm e}^{-{\rm i}H_{\rm mol}t/\hbar}$, and $\sigma_x(t=0) = \sigma_x$. The equation can be simplified further, i.e.

$$C_{\mu\mu}(t) = {\rm Tr}({\rm e}^{{\rm i}H_g t/\hbar}{\rm e}^{-{\rm i}H_e t/\hbar}). \tag{7}$$

The absorption spectrum of molecule $\sigma_{\rm abs}(\omega)$ can be obtained by the Fourier transform of the dipole correlation function, i.e.

$$\sigma_{\rm abs}(\omega) = \int_{-\infty}^{\infty} {\rm d}t\ {\rm e}^{{\rm i}\omega t}\ C_{\mu\mu}(t). \tag{8}$$

Therefore the remaining problem is how to calculate time correlation function.

The working mechanism of our superconducting simulator is summarized as follows (see Fig. 1b and c). First, the qubit is initialized to the ground state $|g\rangle$ while the phonons (cavity) are prepared in a certain given state $|\psi\rangle$ for the purpose of simulating the molecular system initially at different nuclear states. In our experiment, we have prepared different phonon states: (1) a vacuum state at zero temperature, (2) a Fock state $|1\rangle$, (3) a thermal equilibrium state, and (4) a vacuum state with damping. As an example, the pulse sequence for the case of a Fock state $|1\rangle$ is presented in the Supplementary data. The qubit is then through a classical microwave pulse turned into a superposition state $(|g\rangle + |e\rangle)/\sqrt{2}$, after applying a $\pi/2$ rotation, i.e. a Hadamard transformation ${\rm H} \equiv \frac{1}{\sqrt{2}}(|g\rangle + |e\rangle)\langle g| + \frac{1}{\sqrt{2}}(|g\rangle - |e\rangle)\langle e|$.

Next, a controlled-operation $U_{\rm ctrl}$ is applied to the qubit-phonon system, which drives the evolution of the phonons only if the qubit is in $|g\rangle$, i.e.,

$$U_{\rm ctrl} = |g\rangle\langle g| \otimes U(t) + |e\rangle\langle e| \otimes I, \tag{9}$$

where the unitary operator

$$U(t) \equiv {\rm e}^{{\rm i}H_g t/\hbar}{\rm e}^{-{\rm i}H_e t/\hbar}, \tag{10}$$

first evolves the phonons for a time interval t with Hamiltonian H_e, followed by an inverse time evolution with H_g for the same time interval. The operation $U(t)$ can be simplified as follows: in the second quantized form, $p = {\rm i}\sqrt{m\hbar\omega_0/2}(a^\dagger - a)$ and $q = \sqrt{\hbar/2m\omega_0}(a + a^\dagger)$, and we have the Hamiltonian,

$$H_g = \hbar\omega_0 a^\dagger a, \tag{11}$$

and

$$H_e = \hbar\omega_0 b^\dagger b + \hbar\omega_{eg}, \tag{12}$$

describing a harmonic oscillator with an equilibrium position shifted by d relative to H_g. Here

$$b = \mathscr{D}(-\tilde{d})a\mathscr{D}(\tilde{d}) = a + \tilde{d}, \tag{13}$$

with $\tilde{d} = d\sqrt{m\omega_0/2\hbar}$, and $\mathscr{D}(\tilde{d}) = {\rm e}^{\tilde{d}a^\dagger - \tilde{d}^\star a}$ is a displacement operator for single mode. $D = \tilde{d}^2$ is a dimensionless factor, which is known as Huang-Rhys parameter. Consequently, the operator $U(t)$ can be implemented as a displacement operator,

$$U(t) = {\rm e}^{-{\rm i}\phi(t)}\mathscr{D}\Big(\tilde{d}({\rm e}^{{\rm i}\omega_0 t} - 1)\Big), \tag{14}$$

apart from a phase factor ${\rm e}^{-{\rm i}\phi(t)}$, where $\phi(t) \equiv \omega_{eg}t + \tilde{d}^2\sin\omega_0 t$ (see the Supplementary data for derivation details).

Note that this phase factor cannot be ignored, as it yields a relative phase instead of global phase with $U_{\rm ctrl}$. Experimentally, the phase ϕ is realized in the previous $\pi/2$ rotation as an azimuth angle in the X-Y plane on the Bloch sphere (Fig. 1c). The controlled displacement operation $\mathscr{D}^g(\boldsymbol{\alpha})$, effective only when the qubit is at $|g\rangle$ state as indicated by an extra superscript g, is implemented by a broad selective pulse with a Gaussian envelope truncated to $4\sigma = 1.34\ \mu s$ (Fig. 1c). Here the displacement vector $\boldsymbol{\alpha} = \tilde{d}({\rm e}^{{\rm i}\omega_0 t} - 1)$. It is worth noting that the decoherence of the system during this long selective pulse lowers the subsequent qubit measurement contrast by a factor of about 0.83 compared to the ideal case (see the Supplementary data).

Finally, as a result the dipole correlation function, defined as

$$\begin{aligned} C_{\mu\mu}(t) &= \langle\psi|U(t)|\psi\rangle \\ &= {\rm e}^{-{\rm i}\omega_{eg}t - {\rm i}\tilde{d}^2\sin\omega_0 t}\langle\psi|\mathscr{D}(\tilde{d}({\rm e}^{{\rm i}\omega_0 t} - 1))|\psi\rangle \end{aligned} \tag{15}$$

is encoded in the off-diagonal elements of the reduced density matrix of the qubit, i.e.,

$$C_{\mu\mu}(t) = \langle\sigma_x(t)\rangle + {\rm i}\langle\sigma_y(t)\rangle. \tag{16}$$

where $\langle\sigma_y(t)\rangle$ and $\langle\sigma_x(t)\rangle$ of the qubit can be measured by applying an extra $\pi/2$ rotations along X and Y axis ($R_{X\text{ or }Y}$) respectively followed by a Z-basis measurement. More precisely, $R_X \equiv \frac{1}{\sqrt{2}}(|g\rangle - {\rm i}|e\rangle)\langle g| + \frac{1}{\sqrt{2}}(|e\rangle - {\rm i}|g\rangle)\langle e|$ and $R_Y \equiv \frac{1}{\sqrt{2}}(|g\rangle + |e\rangle)\langle g| + \frac{1}{\sqrt{2}}(|e\rangle - |g\rangle)\langle e|$. This general procedure is applicable for any initial state of the phonon, pure or mixed. The absorption spectrum $\sigma_{\rm abs}$ is finally obtained by a Fourier transform of $C_{\mu\mu}(t)$.

We follow the above procedure to simulate the molecular system initially at a vacuum state and a Fock state $|1\rangle$ at zero temperature. However, in order to simulate molecular spectra with the phonon mode initialized in a thermal state, $\rho \equiv {\rm e}^{-\hbar\omega_0 a^\dagger a/kT}/{\rm Tr}({\rm e}^{-\hbar\omega_0 a^\dagger a/kT})$, it is not practical to increase the physical temperature, as the performance of the experimental system would decrease significantly. One way to create a thermal state is to drive the phonon mode with an uncorrelated noise source [47]. Our procedure will then apply directly to such a thermal initial state without any justification. For simplification of experiment and as a proof of concept experiment, here we instead use a classical calculation (not assumed to be scalable) to replace the desired evolution of the phonon system by modifying the

above procedure at Step 1: rather than an equal superposition (after a Hadamard gate), the qubit is initialized to $e^{-i\phi(t)}\sin\frac{\gamma(t)}{2}|g\rangle+\cos\frac{\gamma(t)}{2}|e\rangle$, where the angle $\gamma(t)$ is chosen such that $\sin\gamma=e^{2\bar{d}^2\bar{n}(\cos\omega_0 t-1)}$ and $\bar{n}=(e^{\hbar\omega_0/kT}-1)^{-1}$ (see the Supplementary data).

Similarly, for the case of a vacuum state with damping, we choose $\sin\gamma(t)=e^{-t/\tau}$, where τ is the characteristic time (also see the Supplementary data). In both cases, following the same remaining procedure as described above, one can obtain the correlation function $C_{\mu\mu}^{\rm thm}(t)$ for an initial thermal state and the damped correlation function $C_{\mu\mu}^{\rm damp}(t)=e^{-t/\tau}C_{\mu\mu}(t)$, respectively.

4. Experimental results

Our experimental results are as follows. In our quantum simulation, we have set $\Delta t=1,\ t_{\max}=900,\ \omega_{eg}=\pi/5$, and $\omega_0=\pi/90$, fulfilling the condition $\omega_0\ll\omega_{eg}$. We follow the simulation procedure described previously by varying the qubit rotation angle ϕ and the vector $\boldsymbol{\alpha}$ in the controlled displacement operation (Fig. 1c) to get the time-correlation function $C_{\mu\mu}(t)$ (Eq. (16)) and then its Fourier transform for the absorption spectrum. The spectrum lineshape of molecule illustrates the relative probability of electronic transition between different vibrational states in nuclear space. In Fig. 2, we present the progression of absorption peaks for the case where the phonon state is initialized at vacuum and at zero temperature, i.e. $|\psi\rangle=|0\rangle$, for various Huang-Rhys parameter D. Theoretically, for a vacuum state,

$$C_{\mu\mu}(t)=e^{-i\omega_{eg}t}e^{\bar{d}^2(e^{-i\omega_0 t}-1)},\tag{17}$$

and by Fourier transforming this equation we can obtain the lineshape

$$\sigma_{abs}(\omega)=e^{-D}\sum_{j=0}^{\infty}\frac{1}{j!}D^j\delta(\omega-\omega_{eg}-j\omega_0).\tag{18}$$

The peak intensities are proportional to the square of the overlap between the nuclear vibrational states in the ground and excited states and thus dependent on D, which is a measure of the coupling strength between nuclear and electronic degrees of freedom.

When $D=0$, there is only a sharp peak located at the frequency $\omega=\omega_{eg}$. This case represents the limit where the electronic transition and the nuclear motion are decoupled. In other words, the molecule is essentially the same as a two-level atom, as far as the spectrum is concerned. When D is increased from zero to, e.g., $D=1$, several peaks emerge, and these peaks are equally spaced by the phonon frequency ω_0. When D is increased further to $D=4$, we can observe more equally-spaced peaks. However, the amplitude of the direct transition at $\omega=\omega_{eg}$ is no longer the largest. In all experimental trials, except for a reduction factor $f=0.83$ mainly due to the qubit decoherence, the spectral peaks are in good agreement with the expected Poisson distribution (see the Supplementary data).

The absorption spectrum of the other three different initial nuclear states in the molecular system are shown in Fig. 3: (1) Fock state $|1\rangle$ with different D; (2) thermal equilibrium state at different temperatures characterized by the occupation number $\bar{n}$; and (3) damped vacuum state with different dissipation rates described by the characteristic time τ. The corresponding electronic transitions for each case have been depicted in the top diagrams of Fig. 3. Under all reasonable conditions, the molecular system will

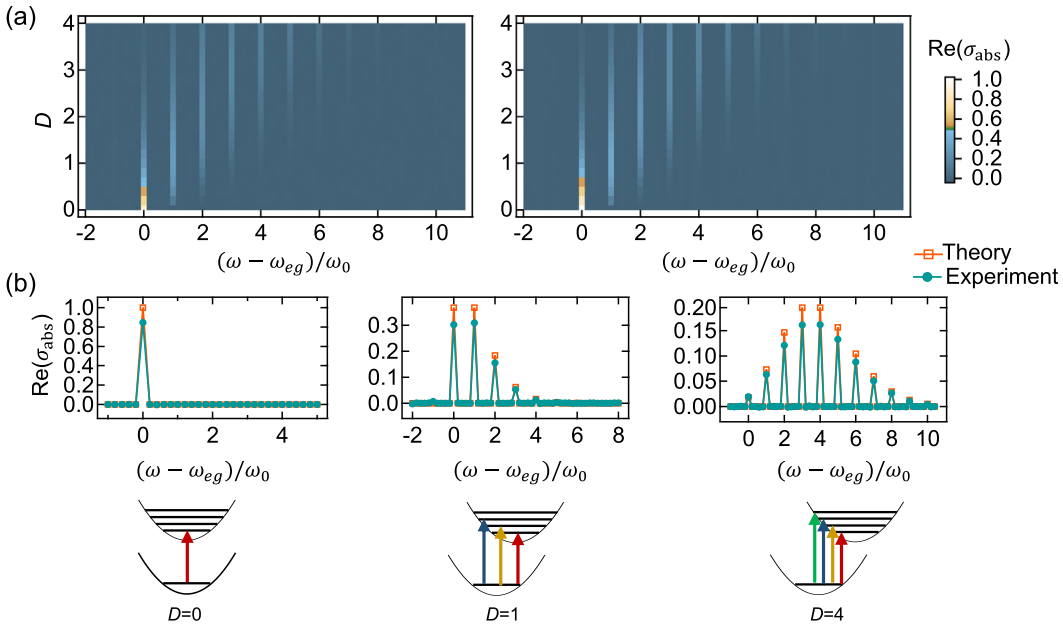

Fig. 2. (Color online) Absorption spectrum of the nuclear system at vacuum ($|\psi\rangle=|0\rangle$) at zero temperature. (a) Progression of the absorption spectrum $\sigma_{\rm abs}$, obtained by a Fourier transform of the time-correlation function $C_{\mu\mu}(t)$ (Eq. (16)), as a function of Huang-Rhys parameter $D=\bar{d}^2$. $C_{\mu\mu}(t)$ is experimentally simulated by varying the qubit rotation angle $\phi=\omega_{eg}t+\bar{d}^2\sin\omega_0 t$ and the vector $\boldsymbol{\alpha}=\bar{d}(e^{i\omega_0 t}-1)$ in the controlled displacement operation as shown in Fig. 1c. Here we only present the real part of $\sigma_{\rm abs}$. The x axis represents the normalized spectral frequency of electronic transition, which describes the necessary energy for transitions from the electronic ground state to the excited states. We compare experimental results (left) with theory (right) using the same color scale which represents the transition probability. (b) The cross section at $D=0$, 1, and 4, and the corresponding schematics of the electronic transitions (bottom row). The peak intensities are proportional to the square of the overlap between the nuclear vibrational states in the ground and excited states and thus dependent on D, which is a measure of the coupling strength between nuclear and electronic degrees of freedom. For $D\ll1$ (weak coupling), the dependence of the energy potentials on the nuclear configuration q is weak and the absorption maximum is at ω_{eg}. For $D\gg1$ (strong coupling), the transition with the maximum intensity is found for peak near $\omega_{eg}+D\omega_0$. As expected, the absorption peaks of zero-temperature molecular spectrum arises from ω_{eg}, separated by ω_0 with a Poisson distribution of intensities (with a mean value D). Here the spectra show only one point as a peak because in this simulation we have intentionally measured an integer number of periods (see the main text). A damping factor will be applied to emulate spectral broadening later. The experimental data are lower by a constant reduction factor $f=0.83$ than theory, as expected dominantly due to the decoherence of the qubit during the simulation process.

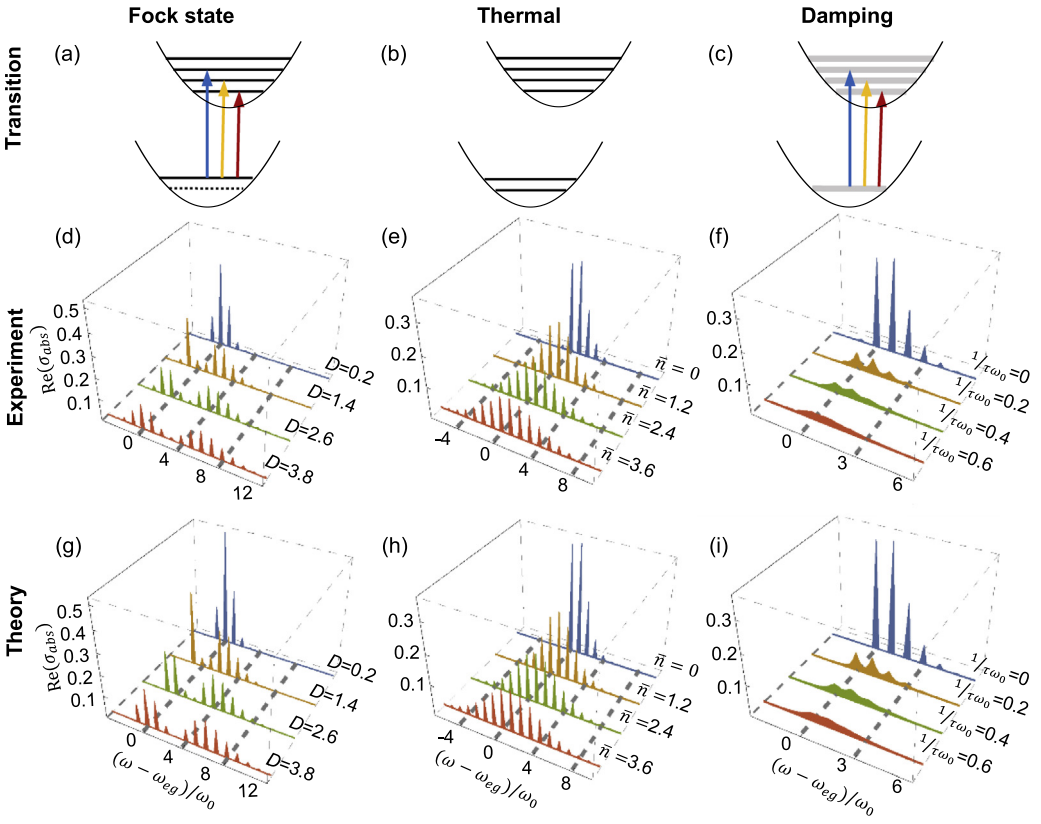

Fig. 3. (Color online) Absorption spectrum of three different initial nuclear states in the molecular system vs different parameters. The top diagrams depict the corresponding electronic transitions: (a) Fock state $|1\rangle$, a non-equilibrium state; (b) thermal state, an equilibrium state; (c) damped vacuum state, with a damping factor to emulate the spectral broadening. (d), (e), (f) and (g), (h), (i) show the corresponding experimental results and theoretical expectations, respectively. For clarity, here we only show the typical spectrums with the corresponding parameter next to each plot. For both thermal state and damped vacuum state, $D = 1$. Except for a reduction of experimental peak values, the experimental results show good agreement with theoretical expectation.

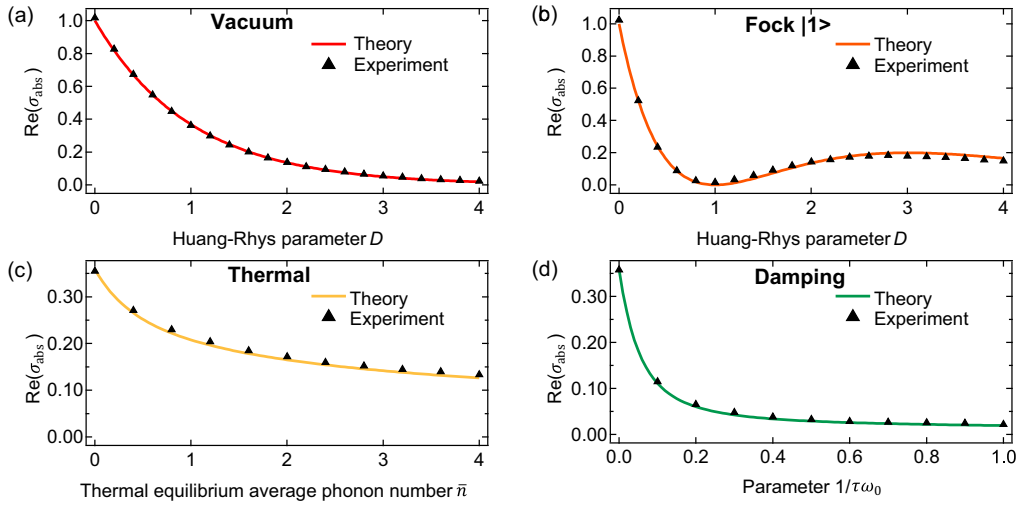

Fig. 4. (Color online) Progression of spectral peak at $\omega = \omega_{eg}$. Peak values at $\omega = \omega_{eg}$ in Figs. 2 and 3 as a function of (a) D for an initial vacuum state; (b) D for a Fock state $|1\rangle$; (c) $\bar{n}$ for a thermal equilibrium state; (d) $1/\tau\omega_0$ for a damped vacuum state. These values characterize the transition probability between molecular electronic ground and excited states at the specific frequency. Dots are experimental data after divided by a constant reduction factor f, in good agreement with theoretical expectation depicted in solid curves. $f = 0.83$ for (a), (c), and (d) while $f = 0.75$ for (b). The smaller f for the case of Fock state $|1\rangle$ is mainly due to the finite Fock state preparation fidelity $F = 0.94$ while all other three cases start from a nearly perfect vacuum state. The standard deviation for each measured value is much less than 0.01 and not shown in the figure.

only be on the ground electronic state without stimulation. The correlation function basically describes the time-dependent overlap of the initial nuclear wave function in the ground state with the time-evolution of the same wave function when initially projected onto the excited state. For clarity, we only show the typical spectra. Except for a reduction of experimental peak values, the experimental results show good agreement with theoretical expectation.

One of the key features of our quantum simulator is that the parameters, such as Huang-Rhys parameter D, can be varied continuously. To better illustrate the progression of the spectrum in Figs. 2 and 3 as a function of various parameters, we present the peak values at $\omega = \omega_{eg}$ as an example in Fig. 4. Dots are experimental data by our quantum simulator while the solid curves represent theoretical expectation. After taking into account the reduction of experimental peak values, again mainly due to the system decoherence, through a division by a constant reduction factor f ($f = 0.83$ for Fig. 4a–d; $f = 0.75$ for Fig. 4b), the experimental results are in good agreement with theoretical expectations. The smaller f for the case of Fock state $|1\rangle$ is mainly due to the finite Fock state preparation fidelity $F = 0.94$ (measured Wigner function shown in the Supplementary data) while all other three cases start from a nearly perfect vacuum state. Note that $f = 0.83$ and $f = 0.75$ will only affect the absorption amplitudes rather than the peak positions.

5. Discussion

Our approach can be scaled up for molecules with multiple vibronic modes. In this case, the dipole correlation function comes from the contributions of the individual modes, i.e., for n modes,

$$C_{\mu\mu}(t) = \left|\mu_{eg}\right|^2 \mathrm{e}^{-\mathrm{i}\left(E_e - E_g\right)t/\hbar} F_n(t), \tag{19}$$

where $F_n(t) = \mathrm{Tr}(\mathrm{e}^{\mathrm{i}H_g^S t/\hbar}\mathrm{e}^{-\mathrm{i}H_e^S t/\hbar}\rho_1 \otimes \rho_2 \cdots \otimes \rho_n)$. Here H_g^S and H_e^S are the sum of H_g^i and H_e^i for the i-th mode, and ρ_i is the corresponding vibrational state. As a result, the superconducting qubit needs to be coupled with multiple cavity modes. In a 3D circuit QED architecture this direction has been realized experimentally [48] and more complex quantum systems can be even further scaled up with a multilayer integrated platform [49]. Note that error propagation in this multi-mode case may be complicated and hard to estimate, which requires a further investigation.

As mentioned before, our current small-scale experiment has not been able to demonstrate advantages over classical simulation. In the future, when the experimental setup is upgraded, there are various ways to achieve advantages over classical simulation: (1) For the moment, the molecular Hamiltonian considered is diagonal in the σ_z basis of the qubit (electronic) system. However, if we are to consider larger molecules, e.g., linear molecular chain, it is possible that a local excitation would propagate to other sites. In this case, the dynamics is highly non-trivial for classical computation. (2) The reason that the correlation function can be determined classically is because it deals with the simple initial phonon states. In principle, one can prepare quantum mechanically an initial phonon state with a large number of superposition of Fock states. For example, the molecule might have a collision with another molecule, so that the phonon state is excited. With a quantum simulator, the complexity in obtaining the spectrum is not changed, but it may take long time to calculate the correlation function classically. (3) One may include a non-linear term to better approximate the energy surface. To do so, we will need to introduce terms containing more bosonic operators, e.g., $a^\dagger a^\dagger aa$, in the Hamiltonian. At the moment, this direction is still under investigation.

On the other hand, the scaling requirement are as follows. Classically, one would generally require to store all the phonon excitations. The scaling is exponential for classical computers. For each mode, if we keep n lowest energy levels, then we need $O(n^m)$ amount of memory for m different modes. For example, if we keep $n = 10$ levels, and $m = 10$, it requires to store 10^{10} states. We expect such extension is within the reach of current superconducting technology.

6. Conclusion

To conclude, we demonstrated experimentally a new method to simulate electronic absorption spectra of a diatomic molecule, where the nuclear vibrational states may or may not be in thermal equilibrium. Our quantum simulator is based on a superconducting circuit QED architecture with flexible parameter tunability. The simulation results indicate that the resulting molecular spectra are in good agreement with theoretical expectation. Finally, we note that this method can be readily extended to other quantum simulation platform, including photonic [50] or trapped-ion [51] systems. Therefore, our experiment represents the beginning of a new approach of predicting molecular spectroscopy using quantum simulators.

Conflict of interest

The authors declare that they have no conflict of interest.

Acknowledgments

MY acknowledges the Guangdong Innovative and En-trepreneurial Research Team Program (2016ZT06D348), and the Science Technology and Innovation Commission of Shenzhen Municipality (ZDSYS20170303165926217 and JCYJ20170412152620376). LS acknowledges the support from the National Natural Science Foundation of China (11474177) and the 1000 Youth Fellowship Program in China. LS also thanks R. Vijay and his group for the help with the parametric amplifier measurements.

Appendix A. Supplementary data

Supplementary data associated with this article can be found, in the online version, at https://doi.org/10.1016/j.scib.2018.02.001.

References

[1] Feynman RP. Simulating physics with computers. Int J Theor Phys 1982;21:467–88.
[2] Kroto Harold W. Molecular rotation spectra. Dover; 1992.
[3] Aspuru-Guzik A, Dutoi AD, Love PJ, et al. Simulated quantum computation of molecular energies. Science 2005;309:1704–7.
[4] Kassal I, Whitfield JD, Perdomo-Ortiz A, et al. Simulating chemistry using quantum computers. Ann Rev Phys Chem 2011;62:185–207.
[5] Whitfield JD, Biamonte J, Aspuru-Guzik A. Simulation of electronic structure Hamiltonians using quantum computers. Mol Phys 2011;109:735–50.
[6] Jones NC, Whitfield JD, McMahon PL, et al. Faster quantum chemistry simulation on fault-tolerant quantum computers. New J Phys 2012;14:115023.
[7] Babbush R, McClean J, Wecker D, et al. Chemical basis of Trotter-Suzuki errors in quantum chemistry simulation. Phys Rev A 2015;91:022311.
[8] Li Z, Yung MH, Chen H, et al. Solving quantum ground-state problems with nuclear magnetic resonance. Sci Rep 2011;1:88.
[9] Lanyon BP, Whitfield JD, Gillett GG, et al. Towards quantum chemistry on a quantum computer. Nat Chem 2010;2:106.
[10] Du J, Xu N, Peng X, et al. NMR implementation of a molecular hydrogen quantum simulation with adiabatic state preparation. Phys Rev Lett 2010;104:030502.
[11] Wang Y, Dolde F, Biamonte J, et al. Quantum simulation of helium hydride cation in a solid-state spin register. ACS Nano 2015;9:7769–74.
[12] Kandala A, Mezzacapo A, Temme K, et al. Hardware-efficient variational quantum eigensolver for small molecules and quantum magnets. Nature 2017;549:242.

[13] Yung MH, Casanova J, Mezzacapo A, et al. From transistor to trapped-ion computers for quantum chemistry. Sci Rep 2014;4:3589.
[14] Peruzzo A, McClean J, Shadbolt P, et al. A variational eigenvalue solver on a photonic quantum processor. Nat Commun 2014;5:4213.
[15] Shen Y, Zhang X, Zhang S, et al. Quantum implementation of the unitary coupled cluster for simulating molecular electronic structure. Phys Rev A 2017;95:020501.
[16] O'Malley PJJ, Babbush R, Kivlichan ID, et al. Scalable quantum simulation of molecular energies. Phy Rev X 2016;6:031007.
[17] Colless J, Ramasesh V, Dahlen D, et al. Implementing a variational quantum eigensolver using superconducting qubits. In Quantum Information and Measurement (QIM) 2017, Page QF6A.2. Optical Society of America, 2017.
[18] Improta R, Barone V, Santoro F. Ab initio calculations of absorption spectra of large molecules in solution: Coumarin C153. Angew Chem 2007;119:409–12.
[19] Houck AA, Tàureci HE, Koch J. On-chip quantum simulation with superconducting circuits. Nat Phys 2012;8:292–9.
[20] Huh J, Guerreschi GG, Peropadre B, et al. Boson sampling for molecular vibronic spectra. Nat Photon 2015;9:615–20.
[21] Aaronson S, Arkhipov A. The computational complexity of linear optics. Theor Comput 2013;9:143–252.
[22] Peropadre B, Guerreschi GG, Huh J, et al. Proposal for microwave boson sampling. Phys Rev Lett 2016;117:140505.
[23] Peng Q, Yi Y, Shuai Z, et al. Toward quantitative prediction of molecular fluorescence quantum efficiency: role of Duschinsky rotation. J Am Chem Soc 2007;129:9333–9.
[24] Bunyk PI, Hoskinson E, Johnson MW, et al. Architectural considerations in the design of a superconducting quantum annealing processor. IEEE Trans Appl Supercond 2014;24:1700110.
[25] Olivares DG, Peropadre B, Huh J, et al. Quantum emulation of molecular force fields: a blueprint for a superconducting architecture. Phys Rev Appl 2017;8:064008.
[26] Mukamel S. Principles of nonlinear optical spectroscopy. Oxford University Press on Demand; 1999.
[27] Fantz U, Wunderlich D. Franck Condon factors, transition probabilities, and radiative lifetimes for hydrogen molecules and their isotopomeres. Atom Data Nucl Data Table 2006;92:853–973.
[28] Knill E, Laflamme R. Power of one bit of quantum information. Phys Rev Lett 1998;81:5672.
[29] Pedernales JS, Di Candia R, Egusquiza IL, et al. Efficient quantum algorithm for computing n-time correlation functions. Phys Rev Lett 2014;113:020505.
[30] Wallraff A, Schuster DI, Blais A, et al. Circuit quantum electrodynamics: coherent coupling of a single photon to a Cooper pair box. Nature 2004;431:162.
[31] Paik H, Schuster DI, Bishop LS, et al. Observation of high coherence in Josephson junction qubits measured in a three-dimensional circuit QED architecture. Phys Rev Lett 2011;107:240501.
[32] Hofheinz M, Weig EM, Ansmann M, et al. Generation of Fock states in a superconducting quantum circuit. Nature 2008;454:310–4.
[33] Hofheinz M, Wang H, Ansmann M, et al. Synthesizing arbitrary quantum states in a superconducting resonator. Nature 2009;459:546–9.
[34] Ben-Kish A, DeMarco B, Meyer V, et al. Experimental demonstration of a technique to generate arbitrary quantum superposition states of a harmonically bound spin-1/2 particle. Phys Rev Lett 2003;90:037902.
[35] Zhang J, Um M, Lv D, et al. Experimental preparation of high NOON states for phonons. arXiv:1611.08700, 2016.
[36] Sundaresan NM, Liu Y, Sadri D, et al. Beyond strong coupling in a multimode cavity. Phys Rev X 2015;5:021035.
[37] Salathe Y, Mondal M, Oppliger M, et al. Digital quantum simulation of spin models with circuit quantum electrodynamics. Phys Rev X 2015;5:021027.
[38] Barends R, Lamata L, Kelly J, et al. Digital quantum simulation of fermionic models with a superconducting circuit. Nat Commun 2015;6:7654.
[39] Barends R, Shabani A, Lamata L, et al. Digitized adiabatic quantum computing with a superconducting circuit. Nature 2016;534:222.
[40] Langford NK, Sagastizabal R, Kounalakis M, et al. Experimentally simulating the dynamics of quantum light and matter at ultrastrong coupling. arXiv:1610.10065, 2016.
[41] Hatridge M, Vijay R, Slichter DH, et al. Dispersive magnetometry with a quantum limited SQUID parametric amplifier. Phys Rev B 2011;83:134501.
[42] Roy T, Kundu S, Chand M, et al. Broadband parametric amplification with impedance engineering: beyond the gain-bandwidth product. Appl Phys Lett 2015;107:262601.
[43] Kamal A, Marblestone A, Devoret M. Signal-to-pump back action and self-oscillation in double-pump Josephson parametric amplifier. Phys Rev B 2009;79:184301.
[44] Murch KW, Weber SJ, Macklin C, et al. Observing single quantum trajectories of a superconducting quantum bit. Nature 2013;502:211.
[45] Liu K, Xu Y, Wang W, et al. A twofold quantum delayed-choice experiment in a superconducting circuit. Sci Adv 2017;3:e1603159.
[46] Wang W, Hu L, Xu Y, et al. Converting quasiclassical states into arbitrary fock state superpositions in a superconducting circuit. Phys Rev Lett 2017;118:223604.
[47] Sears AP, Petrenko A, Catelani G, et al. Photon shot noise dephasing in the strong-dispersive limit of circuit qed. Phys Rev B 2012;86:180504(R).
[48] Wang C, Gao YY, Reinhold P, et al. A Schrödinger cat living in two boxes. Science 2016;352:1087–91.
[49] Brecht T, Pfaff W, Wang C, et al. NPJ Quantum Inf 2016;2:16002.
[50] Aspuru-Guzik A, Walther P. Photonic quantum simulators. Nat Phys 2012;8:285–91.
[51] Kim K, Chang MS, Korenblit S, et al. Quantum simulation of frustrated Ising spins with trapped ions. Nature 2010;465:590–3.